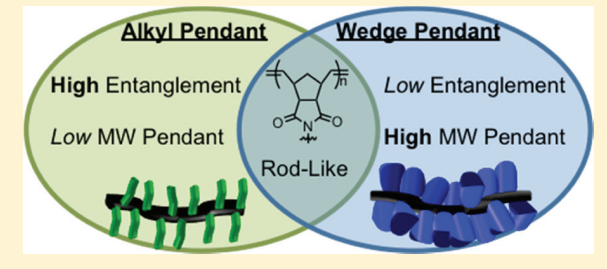
Cite This: Macromolecules XXXX, XXX, XXX–XX

# Impact of the Pendant Group on the Chain Conformation and Bulk Properties of Norbornene Imide-Based Polymers

Bret M. Boyle, †,§ Ozge Heinz, ‡,§ Garret M. Miyake, \*,† and Yifu Ding\*,‡ and Yifu Ding\*,

Supporting Information

**ABSTRACT:** Three series of well-defined norbornene imide-based polymers with different pendant groups were synthesized to investigate the effect of the pendant group on the polymer conformation in solution and bulk melt properties. Each of these three series was examined by analyzing the polymers' bulk *z*-average radius of gyration via static light scattering and the polymers' melt viscoelastic properties via oscillatory measurements and differential scanning calorimetry. Sterically bulky pendant wedge groups modestly increase the rodlike conformation of the norbornene-imide polymer, however, the inherent rigidity of the polymer main-



chain can still be observed with less bulky substituents. In stark contrast, the different side groups significantly impacted the bulk viscoelastic and thermal properties. By increasing the pendant group size, the chain diameter of the polymer increases and lowers the entanglement modulus. Finally, as the wedge pendant group size increases, the segmental relaxation time and the fragility index of these norbornene-based polymers are decreased.

# INTRODUCTION

Bottlebrush polymers are molecules containing densely spaced polymeric side chains grafted onto a central backbone. These densely packed polymeric side chains give a cylindrical conformation to the bottlebrush molecule. It is this cylindrical conformation of bottlebrush polymers that imparts significant influences on the bulk materials properties. 1-4 An increase in grafting density and length of the side chains increases the cross-sectional diameter and persistence length of the brush polymer chains, while also creating a secondary relaxation process and a reduction of the entanglement modulus. 5-8 These unique properties of molecular brush polymers are due to the added degrees of freedom available to the longer side chains, which give rise to more entropically favored conformations compared to shorter side chains. Therefore, the brush backbone adopts a more rodlike shape when paired with longer side chains to help accommodate more favorable side chain conformations. A number of theoretical models have been developed to describe the origin of the differences in physical properties between linear polymers and brush polymers. <sup>9,10</sup> Theories, including the packing model <sup>11,12</sup> and reptation theory, <sup>1,13</sup> have aided in conceptualizing many of the experimental results observed in brush polymers. Two of the most valuable interpretations of these models are in predicting brush polymer conformation and describing the two distinct rheological relaxations of brush polymers.

The polymer architecture described as dendronized polymers, <sup>14</sup> however, has received less attention with respect to the theoretical understanding of their structure and dynamics. Dendronized polymers are polymers with side

groups extending away from the backbone that contain one or more branch points in which another generation of branches begins. Often, these dendronized polymers can be directly polymerized from discrete monomers 15-19 and contain unique chemical<sup>20</sup> and physical properties that have enabled many different, new applications such as gene delivery vectors,<sup>2</sup> stimuli-responsive materials, 22 catalytic frameworks, 23 or polymeric photonic crystals. 8,24,25 Dendronized polymers also present the opportunity to expand polymer physics models to this intermediate regime of polymer architectures due to the facility with which polymer girth and functionality can be tuned. 26-31 Previously, the effects of a large-molecular-weight wedge pendant group on the linear rheological responses of a norbornene imide-based polymer were investigated.<sup>27</sup> Multiple molecular weights of polymers synthesized from an alkyl wedge monomer with three n-dodecyl alkyl chains (DDW) were investigated. This series of wedge polymers exhibited a reduced degree of entanglement as given from a low rubbery plateau modulus value (order of 10<sup>4</sup> Pa) and a low glassy modulus (~10<sup>8</sup> Pa) observed by rheology. Typically, linear polymers exhibit a rubbery plateau modulus value around 10<sup>5</sup>-10<sup>6</sup> Pa and a glassy modulus value around a value of  $10^9 - 10^{10}$  Pa. 32 The study also reported a dynamic fragility value of m = 65 for the DDW polymer, which is consistent with a flexible chain polymer rather than a stiff backbone polymer as might be expected from a norbornene backbone. The relative con-

Received: January 4, 2019 Revised: April 16, 2019

<sup>&</sup>lt;sup>†</sup>Department of Chemistry, Colorado State University, Fort Collins, Colorado 80523, United States

<sup>&</sup>lt;sup>‡</sup>Department of Mechanical Engineering, University of Colorado, Boulder, Colorado 80309, United States

tributions of the pendant group size to the norbornene imide-based polymer properties, however, remain unclear. The work reported herein aims to investigate the effects on the polymer conformation, thermal, rheological, and mechanical properties of polymers possessing dendronized pendant groups of varying sizes at a norbornene imide backbone. The results reveal that the size of the side group appears to less significantly impact the fractal dimensions of the polymer chain but significantly impacts the thermomechanical and dynamic properties of these polymers.

# MATERIALS AND METHODS

The polymers were synthesized by ring opening metathesis polymerization (ROMP) of norbornene-based monomers using a catalyst,  $(H_2IMes)(PPh_3)(Cl)_2RuCHPh$ . The full synthetic procedure is detailed in the Supporting Information. Polymer molecular weight and z-average radius of gyration values were obtained using gel permeation chromatography columns from Agilent coupled with a WYATT miniDAWN TREOS multiangle light scattering detector.

The thermal properties of each polymer were obtained using a TA Instruments thermal gravimetric analyzer (TGA) Q50/Q500 in conjunction with a TA Instruments differential scanning calorimeter (DSC) 2500. The temperature scan of the TGA experiments ranged from 25 to 850 °C at a ramp rate of 10 °C/min. The DSC method contained one temperature sweep to erase the thermal history, which was then followed by a second heating scan from 0 to 150 °C at a ramp rate of 5 °C/min. Further details of each thermal experiment are detailed in the attached Supporting Information.

The viscoelastic measurements were conducted using a TA Instruments Dynamic Mechanical Analyzer (DMA), Q800 V20.26 Build 45, and TA Instruments rheometers, AR-G2 and DHR-2. The DMA was conducted under a constant nitrogen flow with a constant strain of 0.3% over a temperature range of -50-300 °C. The rheometers were outfitted with 8 mm steel parallel plates, and experiments were conducted under a nitrogen atmosphere. The samples were loaded onto the plates and heated until they could be slowly pressed until the gap was approximately 1 mm using axial stress. For testing, the axial stress was equilibrated to  $0.0 \pm 0.2$  N. The dynamic frequency sweeps were performed over a temperature range from 90 to 180 or 50 to 140  $^{\circ}$ C. The frequency range for the dynamic frequency sweep experiments was from 0.01 to 100 rad/s with a 0.1% strain. The time-temperature superposition (TTS) was completed with vertical and lateral shifts within the TA Trios Software. A more detailed and thorough experimental method can be found in the attached Supporting Information document.

# RESULTS AND DISCUSSION

To investigate the effects of the side group on norbornene-based polymers, three different norbornene-based monomers were polymerized using ruthenium-mediated ring-opening metathesis polymerization  $(ROMP)^{33-36}$  to produce a series of polymers possessing degrees of polymerization (DP) through the polymer backbone ranging from oligomeric DPs of 9 up to polymer DPs as high as 9905. The ROMP produced well-defined polymers within each polymer series, accessing a large range of backbone DPs with low dispersity (<1.30) (Tables S1–S3). Each of the three polymer series was chosen to systematically increase the sterics of the side group attached to the norbornene backbone: an n-hexyl side group [p(HNb)], a dendronized group with three ethyl alkyl chains attached [p(EtW)], and a dendronized group with three n-dodecyl alkyl chains attached [p(DDW)] (Scheme 1).

Characteristics of the chain conformation including the scaling factor and fractal dimension can be obtained by comparing the z-average radii of gyration  $(R_z)$  of these polymers in solution to their number-average molecular

Scheme 1. Synthetic Approach to the Linear HNb MW Series (a) and the Ethyl ( $R = C_2H_5$ ) or the Dodecyl ( $R = C_{12}H_{25}$ ) Alkyl Wedge MW Series (b)

weights  $(M_n)$  or their DPs.<sup>37–40</sup> The  $R_z$  and  $M_n$  values of the polymers were determined in tetrahydrofuran using multiangle static light scattering coupled with gel permeation chromatography (GPC–MALS). The slope of the best-fit line of  $R_z$  versus DP corresponds to the scaling factor (f) of the polymer series (Figures 1 and S7). For the p(HNb) polymer

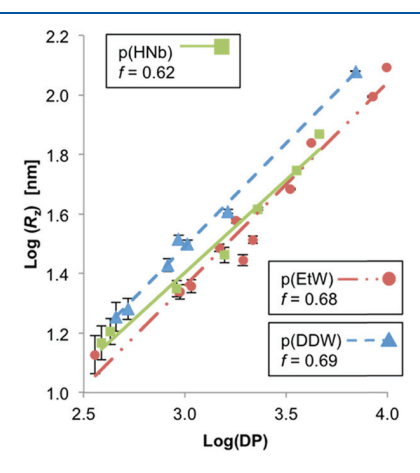


**Figure 1.** Double logarithmic plot of the radius of gyration  $(R_z)$  vs the degree of polymerization (DP) of the p(HNb) series (green squares), the p(EtW) series (red circles), and the p(DDW) series (blue triangles) with the relative uncertainty in  $R_z$  measurements shown with error bars.

series, a scaling factor of  $0.62 \pm 0.04$  was determined, whereas for the wedge polymer series, scaling factors of  $0.68 \pm 0.05$  for the p(EtW) series and  $0.69 \pm 0.03$  for the p(DDW) series were determined (Figure 1). These scaling factors correspond to fractal dimension values ( $f^{-1}$ ) of 1.61 for the p(HNb) series,

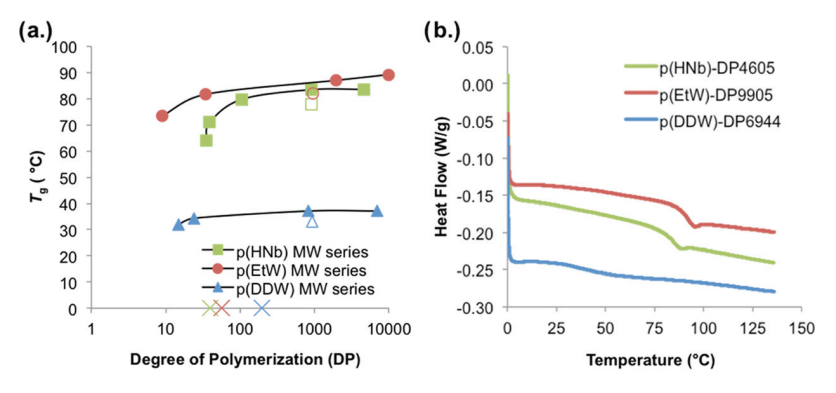


Figure 2. Plot of the  $T_g$  as a function of DP for p(HNb) (green squares), p(EtW) (red circles), and p(DDW) (blue triangles) (a). The DMA  $T_g$  value is shown with unfilled symbols of the respective polymer series (square for p(HNb), circle for p(EtW), and triangle for p(DDW)). The masses of entanglement of each of the series are marked as an "X" in each series' respective color (green for p(HNb), red for p(EtW), and blue for p(DDW)). The lines are used to guide the eyes. The second heating DSC traces (ramp rate of 5 °C/min) for the high-MW polymers in each series are plotted (b).

1.47 for the p(EtW) series, and 1.45 for the p(DDW) series (see p S15 for more details).

The observations of these scaling factors and fractal dimensions are significant for two reasons. First, according to the scaling theory, 41 in a good solvent a rigid-rod polymer theoretically exhibits a scaling factor of 1, whereas a random self-avoiding walk (RSAW) flexible polymer theoretically exhibits a scaling factor of 0.6. 42,43 These scaling factors correspond to a fractal dimension value of 1 for rigid-rod polymers and a value of 1.67 for RSAW polymers. The fractal dimensions of the polymers studied herein are found to have values between the rigid-rod and RSAW polymers and are considered semiflexible. Second, when comparing the fractal dimension of p(HNb), 1.61, to the two wedge polymers' fractal dimensions (1.47 for p(EtW) and 1.45 for p(DDW)), the data suggests that the rigidity of the norbornene-based wedge polymers arises somewhat from the inherent rigidity of the polymer main chain and less than might be expected from the bulkiness of the wedgelike side groups. Further, the bulkiness of the wedge side groups that controls the conformation of the polymer stems from the planar ester and benzene motifs of the side chain rather than the alkyl substituents. This observation is in agreement with the observations often made in brush polymer systems where the longer the side chain, or the greater the radius of gyration of the side chain, the more the rigid-rod character of the polymer conformation. 10,44 This agreement with trends seen in brush polymer systems is further confirmed when comparing the polymer persistent lengths  $(l_p)$  estimated from the  $R_z$  values for each polymer (Tables S7-S9). The expression used to estimate the  $l_p$  is shown below

$$R_z^2 = Ll_p - l_p^2 + \frac{2}{L}l_p^3 - \frac{2}{L^2}(1 - e^{-L/l_p})l_p^4$$
 (1)

where L is the contour length estimated by the product of the degree of polymerization and the backbone monomer size. The p(HNb) with a DP = 912 (pHNb)-DP912 has an estimated  $l_{\rm p}$  of  $1.1\pm0.1$  nm, which is similar to the estimated  $l_{\rm p}$  of the p(EtW)-DP943 at  $1.0\pm0.1$  nm. However, as the side group increases in size to that of the p(DDW) series, so does the  $l_{\rm p}$  as shown by the estimated  $l_{\rm p}$  of p(DDW)-DP930 at 2.3  $\pm$  0.1 nm. The  $l_{\rm p}$  for the p(DDW) is about double the size of the p(HNb) and p(EtW)  $l_{\rm p}$ .

To examine the bulk thermal, mechanical, and rheological properties of these three polymers, we carried out differential scanning calorimetry (DSC), dynamic mechanical analysis (DMA), and rheological measurements. Figure 2a plots the glass transition temperature  $(T_g)$  values, determined by DSC, as a function of DP for the three polymer series studied. All three polymers showed an increase of  $T_g$  with DP at low molecular weights (4-21 kg/mol) and approached their respective asymptotic values. This trend is similar to that of conventional linear polymers and can be rationalized by either conformational entropy theory or chain-end free volume arguments. 45 Among the three series, p(HNb) exhibited the most dramatic decrease in  $T_{\sigma}$  with the reduction in DP at lowmolecular-weight regimes. For p(HNb) and p(EtW), the asymptotic  $T_g$  values were 84 and 89 °C, respectively. Clearly, the replacement of hexyl side group with ethyl wedge did not significantly affect the segmental relaxation process. In contrast, the asymptotic  $T_g$  value of p(DDW) was 38 °C, nearly 50 °C below that of the other two polymers. The significant reduction of  $T_g$  in p(DDW) can be attributed to the internal plasticization effect caused by the flexible n-dodecyl side groups, as commonly observed for other polymers, such as poly(n-alkyl methacrylates). 46,47 As such, the C<sub>12</sub> alkyl groups on the wedge side group significantly enhanced the segmental relaxation, in contrast to their negligible impact on the chain dimensionality.

Additionally, the DP corresponding to the entanglement molecular weight  $(M_{\rm e})$ , obtained from the rheological characterization below, is also marked in Figure 2a. The leveling-off of the  $T_{\rm g}$  values may only be related to the onset of entanglement in the p(HNb) series but not as apparent in the dendronized polymers. This is in contrast to most linear polymers<sup>48</sup> and warrants further investigation.

To investigate the mechanical properties of these polymers, DMA with a temperature ramp rate of 3 °C/min and a constant strain of 0.3% was performed on p(HNb)-DP912, p(EtW)-DP943, and p(DDW)-DP930, three representative polymers with similar DPs. Figure 3 shows the storage modulus  $(E'(\omega))$ , loss modulus  $(E''(\omega))$ , and  $\tan(\delta)$ , as a function of temperature from DMA measurements under dynamic tensile loading. Similarly to the DSC measurements, the  $T_{\rm g}$  value estimated by DMA, marked by the abrupt drop in  $E'(\omega)$ , for p(DDW)-DP930 (~36 °C) was much lower than p(EtW)-DP943 or p(HNb)-DP912 (~80 °C). Note that these

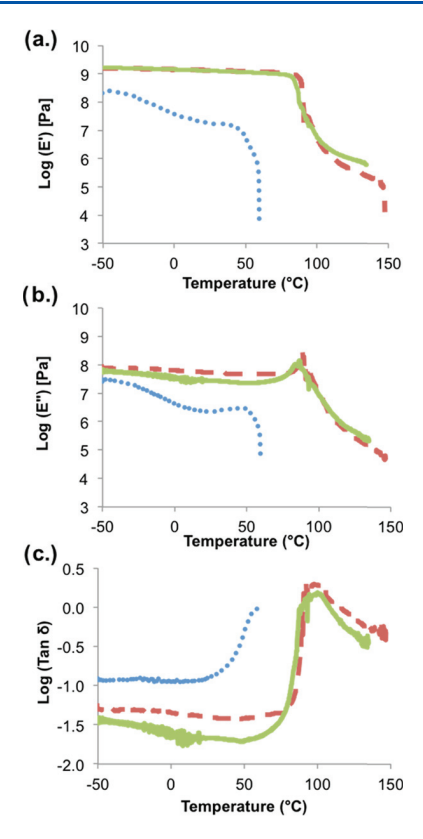


**Figure 3.** Dynamic mechanical responses of the p(HNb)-DP912 (green solid line), p(EtW)-DP943 (red dashed line), and the p(DDW)-DP930 (blue dotted line) are plotted as the storage modulus (a), the loss modulus (b), and the  $\tan\delta$  (c) versus temperature.

values appeared systematically lower than the values obtained from DSC, most likely due to the slower ramp rate of the DMA than that of the DSC. Further, these values were plotted in Figure 2a as a comparison of the  $T_{\rm g}$  values obtained for wellentangled polymer samples by both DSC and DMA techniques.

Figure 3 also shows that p(HNb)-DP912 and p(EtW)-DP943 had very similar glassy modulus values of ~1.5 GPa at -50 °C, which is within the typical range of glassy polymers. However, the glassy modulus of p(DDW)-DP930 at −50 °C was 0.2 GPa, which was nearly 1 order of magnitude lower than those of p(HNb)-DP912 and p(EtW)-DP943. Such an uncommonly low value of glassy modulus for p(DDW) is consistent with the previous report.<sup>27</sup> Moreover, p(DDW)-DP930 showed over a 1 order of magnitude reduction in modulus from 0.2 GPa at -50 °C to 0.014 GPa at 36 °C within the glassy state. Since this behavior was not observed in p(EtW)-DP943, this relaxation process and the corresponding low value of modulus can be attributed to the presence of ndodecyl wedge side groups. Further, such a low glassy modulus is not associated with the presence of a secondary relaxation as the glassy modulus at -110 °C (0.3 GPa) is similar to that of the glassy modulus at -50 °C (0.2 GPa). Instead, the similarity in glassy modulus values at these two temperatures suggests a relatively low degree of packing, potentially in combination with low cohesive forces, of the p(DDW) sample.<sup>8,49,50</sup> At temperatures above the  $T_g$ , both p(HNb)-DP912 and p(EtW)-DP943 showed the presence of the rubbery plateau with modulus ~0.1 MPa, indicating that both polymers were wellentangled. In contrast, the rubbery plateau for p(DDW)-DP930, if present, was challenging to detect under tensile loading.

To investigate the melt dynamics of these polymers, rheological measurements were carried out for the three polymers. Figure 4a shows the dynamic shear storage modulus

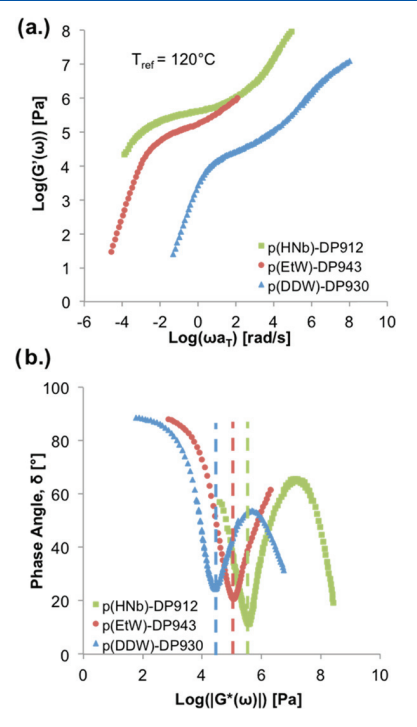


Figure 4. Dynamic storage modulus master curves vs frequency (a) and the van Gurp–Palmen (VGP) traces of phase angle vs complex modulus (b) for the p(HNb)-DP912 (green squares), p(EtW)-DP943 (red circles), and the p(DDW)-DP930 (blue triangles). The dash lines in (b) mark the position of the local minimums.

 $G'(\omega)$  as a function of frequency at the same reference temperature ( $T_{ref}$  = 120 °C), for p(HNb)-DP912, p(EtW)-DP943, and p(DDW)-DP930 (see Figure S27 for the approximately isofrictional master curves). These master curves, covering a window of 8 to 10 orders of magnitude in frequency, were constructed via standard time and temperature superposition (TTS) processes at a reference temperature  $T_{ref}$ = 120 °C. All three polymers displayed characteristic regions similar to those of conventional linear polymers: a glass-torubber transition region at high frequency, a rubbery plateau, and a terminal flow region at low frequency. Despite the similar shape, the master curve of p(DDW)-DP930 shifted to the high-frequency side by nearly 3 orders of magnitude in frequency. This enhanced relaxation rate, especially the segmental relaxation process associated with the glass-torubber transition region, was caused by the much lower  $T_o$ value compared to that of the other two polymers (Figure 2). Furthermore, the rubbery modulus,  $G_N^0$ , for p(DDW)-DP930 was significantly lower than that of the other polymers (vide infra). The chain relaxation time  $(\tau_1)$  marking the onset of the terminal flow regime for the three polymers can be estimated at the crossover frequency  $(G'(\omega) = G''(\omega))$  (Figure 4a).<sup>51</sup> Specifically,  $\tau_1$  was estimated to be 2450, 384, and 0.37 s for p(HNb)-DP912, p(EtW)-DP943, and p(DDW)-DP930 at 120  $^{\circ}$ C, respectively. The much faster  $\tau_1$  for p(DDW)-DP930 is

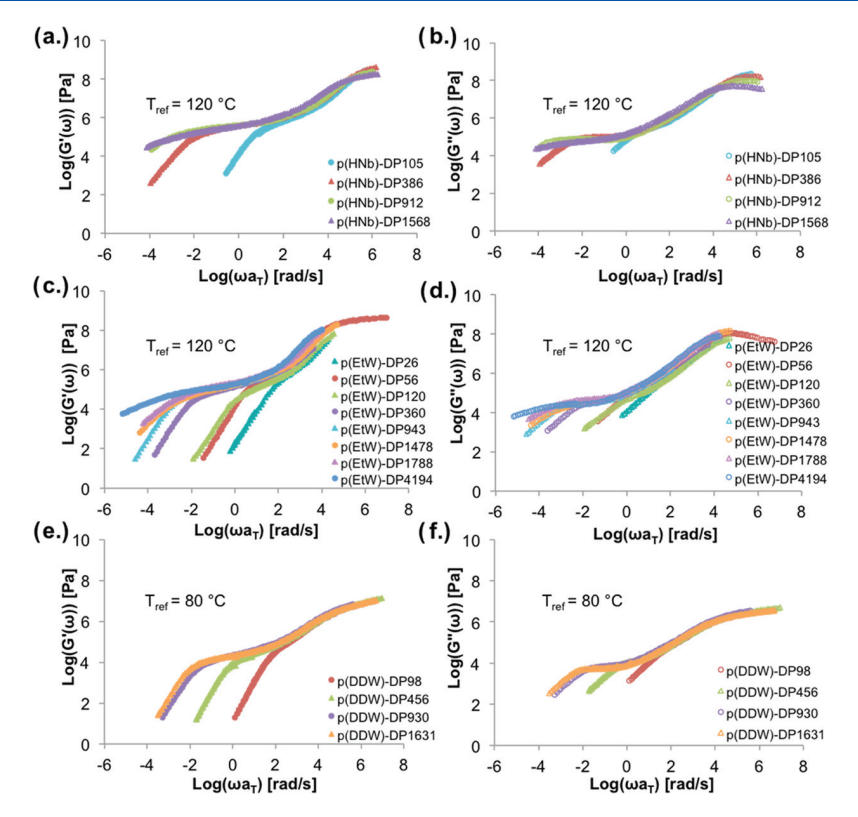


Figure 5. Dynamic master curves for all three polymers that exhibit the storage modulus (a) and loss modulus (b) of the p(HNb) series ( $T_{ref}$  = 120 °C), the storage modulus (c) and the loss modulus (d) of the p(EtW) series ( $T_{ref}$  = 120 °C), and the storage modulus (e) and the loss modulus (f) of the p(DDW) series ( $T_{ref}$  = 80 °C).

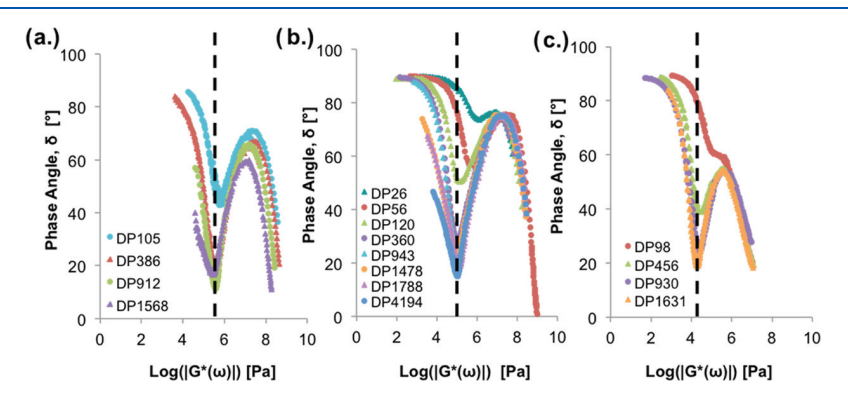


Figure 6. VGP plots of the phase angle versus the magnitude of the complex modulus for the p(HNb) series (a), the p(EtW) series (b), and the p(DDW) series (c). The dashed lines mark the position of the local minima.

mostly attributed to the much faster segmental relaxation process, which sets the monomer friction coefficient that governs the chain relaxation process.

To validate the TTS practice, van Gurp–Palmen (VGP) plots (Figure 4b) were constructed for all three polymers.  $^{52,53}$  The VGP plot, or phase angle ( $\delta$ ) as a function of complex modulus ( $G^*(\omega)$ ), is temperature-invariant (i.e., for each sample, the data was taken at varying temperatures and plotted without any shifts). All three polymers displayed smooth, continuous VGP curves (Figure 4b), which validated the TTS used to construct the master curves in Figure 4a. In addition, the VGP traces of the three polymers show a similar shape: with decreasing  $G^*(\omega)$ , the phase angle first increased to a local maximum, decreased to a local minimum, and finally increased to a plateau of  $90^\circ$ , characteristic of pure viscous behavior. Such an evolution agrees well with the three regions

of relaxation behaviors seen in Figure 4a. The overall shape of the curves matched well with those of conventional monodisperse, linear polymers, but differed from the H-shaped and star-shaped polymers with long side chains. 54

The local minimum in the VGP plots, marked by the dashed lines in Figure 4b, provided a reliable estimation of the plateau modulus,  $G_{\rm N}^{0.49}$ 

$$G_{\mathcal{N}}^{0} = \lim_{\delta \to 0} |G^{*}(\delta)| \tag{2}$$

Accordingly,  $G_N^0$  values were determined to be 3.79  $\times$  10<sup>5</sup>, 1.06  $\times$  10<sup>5</sup>, and 2.57  $\times$  10<sup>4</sup> Pa for p(HNb)-DP912, p(EtW)-DP943, and p(DDW)-DP930, respectively. In addition, the phase angle at the minimum increased as p(HNb)-DP-912 < p(EtW)-DP943 < p(DDW)-DP930. The values of both the phase angle and complex modulus at the minimum indicating the degree of

entanglement and the rubbery elasticity, increased in the order of p(HNb)-DP-912 > p(EtW)-DP943 > p(DDW)-DP930.

To fully understand the influence of the side groups on the melt dynamics, rheological measurements of the three polymer series with varying molecular weights were carried out. Figure 5 shows the dynamic master curves obtained from TTS with  $T_{\rm ref}$  = 120 °C for p(HNb) and p(EtW) and  $T_{\rm ref}$  = 80 °C for p(DDW). An analysis of the horizontal shift factors ( $a_{\rm T}$ ) used to complete these dynamic master curves will be completed following the detailed discussion of the melt dynamics. Note that the lower reference temperature for p(DDW) polymers was adopted to allow comparison with the other two polymer series within the same frequency window, as the  $T_{\rm g}$  values for the p(DDW) series are much lower than those for the other two polymer series (Figure 2).

From Figure 5, polymers with low DPs, e.g., p(EtW)-DP26 and p(DDW)-DP98, showed typical rheological responses of unentangled chains with an absence of a rubbery plateau. With an increase in DP, the rubbery plateaus become more extended and more evident, indicating the formation of entangled, transient polymer networks. Figure 6 shows the VGP plots for all of the polymers, again confirming the validity of TTS used in constructing all of the master curves in Figure 5. VGP plots also showed that the local minimum converged at similar  $G^*(\omega)$  values (marked by the dashed line) with an increase of DP for all three polymer series.

As mentioned earlier,  $G_{\rm N}^0$  can be obtained from the local minimum, which can then be used to estimate the average  $M_{\rm e}$  for each polymer

$$M_{\rm e} = \frac{\rho RT}{G_{\rm N}^0} \tag{3}$$

where  $\rho$  is the polymer melt density at T (e.g.,  $T_{\text{ref}}$  in this case). 27,40 Using the data for the highest DP of each polymer series as they were well entangled,  $G_N^0$  and  $M_e$  values were estimated. Specifically,  $G_N^0$  values for p(HNb)-DP1568, p(EtW)-DP4194, and p(DDW)-DP1631 were determined to be  $2.81 \times 10^5$ ,  $1.03 \times 10^5$ , and  $1.87 \times 10^4$  Pa, respectively. Subsequently,  $M_{\rm e}$  values for p(HNb)-DP1568 ( $T_{\rm ref}$  = 120 °C), p(EtW)-DP4194 ( $T_{ref} = 120$  °C), and p(DDW)-DP1631 ( $T_{ref}$ = 80 °C) were estimated to be  $9.89 \times 10^{3}$ ,  $2.53 \times 10^{4}$ , and 1.71  $\times$  10<sup>5</sup> g/mol, respectively. The  $M_{\rm e}$  value of p(DDW)-DP1631, consistent with the value reported in ref 27, is among the lowest value observed for synthetic polymers.<sup>58</sup> The comparison clearly shows that the increase in the size of the side groups dramatically increases the value of  $M_e$ . Normalized by the molecular weight of the corresponding repeating units  $(M_0)$ , the average number of repeating units between entanglements  $(N_e = M_e/M_0)$  for p(HNb)-DP1568, p(EtW)-DP4194, and p(DDW)-DP1631 were 30, 60, and 198, respectively. Clearly, the dramatic increase in Ne occurred when n-dodecyl wedge side groups replaced the ethyl wedge side groups (Scheme 1).

Figure 7 plots the phase angle at the local minimum  $(\delta_{\rm m})$  as a function of molecular weight, normalized by the value of  $M_{\rm e}$ . Interestingly, the three different polymer series collapsed into a similar dependency in the double logarithmic plot (inset of Figure 7), showing a decrease of  $\delta_{\rm m}$  with an increase of molecular weight. This dependency can be empirically fitted as  $\log(\delta) = 1.74 \times \log(M_{\rm n}/M_{\rm e}) - 0.34$  and suggests that the terminal relaxation is separated from the fast local relaxation with a narrow mode distribution as  $M_{\rm n}/M_{\rm e}$  increases.

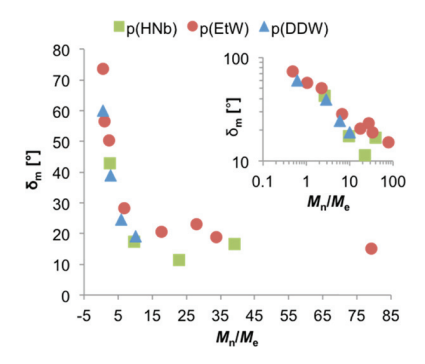
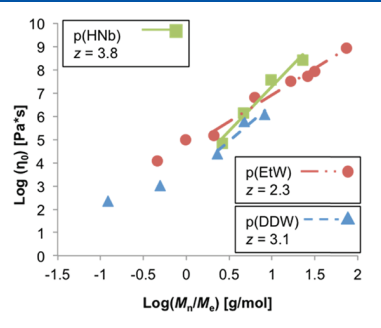


Figure 7. Phase angle at the local minimum  $(\delta_m)$  of the VGP traces (data shown in Figure 6) as a function of molecular weight (normalized by  $M_{\rm e}$  values estimated using the largest DP for each polymer series) for the three series of polymers. The inset shows the same data as that plotted in the double logarithmic plot.

Moreover, Figure 7 suggests that all three types of polymers attained well-entangled behavior (i.e.,  $\delta_{\rm m}$  < 20°) when the molecular weights reached above 10 times the value of  $M_{e}$ which is similar to conventional linear polymers. 53,54 Figure 7 also shows that p(EtW)-DP26 (and DP-56) and p(DDW)-DP98, all of which were below 2Me, were all unentangled as their  $\delta_{\rm m}$  > 45 °C (loss component dominant). This observation was consistent with the absence of rubbery plateaus in their mechanical spectra (Figure 5). It is worth noting that these unentangled chains also displayed a local minimum in the VGP plots, which is most likely attributed to the entropic elasticity of these shorter chains (i.e., the Rouse modes). Such a trend is consistent with the predictions of the packing model: with an increase of chain cross section, the  $M_e$ value increases. This trend is also consistent with the trends seen in bottlebrush polymers and further supports the arguments of the packing model, which states that as the ratio between backbone lengths per unit volume gets smaller, the entanglement decreases. In other words, as the diameter of the polymer chain increases, the entanglement decreases.<sup>11</sup>

For each of the polymer series, at close to isofrictional conditions, Figure 8 shows plots of the zero-shear viscosity  $(\eta_0)$  data against the reduced molecular weight  $(M_{\rm n}/M_{\rm e})$  together with the results of power-law fitting of those data,  $\eta_0 \sim (M_{\rm n}/M_{\rm e})^z$  when  $M_{\rm n}/M_{\rm e} > 2$  with the exponent z as indicated in the legend. The  $\eta_0$  value is estimated from the dynamic modulus master curves using the following equation  $^{26}$ 



**Figure 8.** Double logarithmic plots of the zero shear-rate viscosity  $(\eta_0)$  as a function of molecular weight, normalized by the value of  $M_{\rm e}$  for the p(HNb) series (green squares), the p(EtW) series (red circles) series, and the p(DDW) series (blue triangles) series at a reference temperature close to isofrictional conditions ( $T_{\rm ref} = T_{\rm g} + X$ , where  $X = 36~{\rm ^{\circ}C}$  for p(HNb), 31  ${\rm ^{\circ}C}$  for p(EtW), and 42  ${\rm ^{\circ}C}$  for p(DDW)).

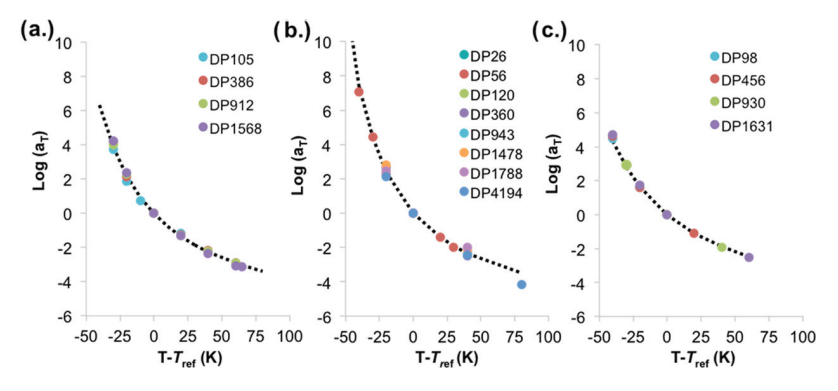


Figure 9. TTS shift factors ( $a_T$ ) used to construct the master curves versus temperature for the p(HNb) MW series (a), the p(EtW) MW series (b), and the p(DDW) MW series (c). The black dashed lines represent WLF fits at a reference temperature close to isofrictional conditions for all three samples ( $T_{ref} = T_g + X$ , where X = 36 °C for p(HNb), X = 31 °C p(EtW), and X = 42 °C for p(DDW)).

$$\eta_0 = \lim_{\omega \to 0} \frac{G''(\omega)}{\omega} \tag{4}$$

The p(HNb) series has z value of 3.8, which resembles the value of 3.4 of an ordinary, linear polymer, but for the p(EtW) and p(DDW) series, the z values were reduced to 2.3 and 3.1, respectively. This drop in z value indicates that the dendronized polymers are less entangled than the standard, linear polymer. It is important to note that the apparent difference between the z values of the p(EtW) and p(DDW) series is most likely due to the shorter  $M_{\rm n}/M_{\rm e}$  range of polymers tested for the p(DDW) series. Further, the p(EtW) and p(DDW) series do not reach the z value of 1 that completely unentangled systems such as polymer brushes or second generation wedges do. Therefore, the z value for the dendronized polymer series plotted in Figure 8 demonstrates further support for the arguments proposing that as the polymer chain diameter is increased, the entanglement decreases.

Figure 9 shows the temperature dependence of  $a_T$  used to construct the master curves shown in Figure 5, which were described by the Williams–Landel–Ferry (WLF) equation<sup>59</sup>

$$\log a_{\rm T} = -\frac{C_{\rm l}(T - T_{\rm ref})}{C_{\rm 2} + T - T_{\rm ref}} \tag{S}$$

with  $T_{\rm ref}=T_{\rm g}+X$  °C to attain close to isofrictional conditions for all three polymer series, where X=36 °C for p(HNb), X=31°C p(EtW), and X=42 °C for p(DDW). Accordingly, the WLF constants for polymers with  $M_{\rm n}$ -independent  $T_{\rm g}$  values,  $C_1$  and  $C_2$ , are listed in Table 1. To further evaluate the

Table 1. WLF Constants Obtained Using Close to Isofrictional Conditions and When  $T_{\text{ref}} = T_{\text{g}}$ 

WLF constants	p(HNb)		p(EtW)		p(DDW)	
$T_{ m ref}$	120 °C	84 °C	120 °C	89 °C	80 °C	38 °C
$C_1$	6.94	12.17	6.82	11.5	6.70	11.4
$C_2$	83.8	47.8	76.7	45.7	102	59.8

temperature dependence of the  $a_{\rm T}$  near the  $T_{\rm g}$  for all three polymer series, the  $C_{\rm 1,g}$  and  $C_{\rm 2,g}$  values were calculated with  $T_{\rm ref}=T_{\rm g}$  for all three polymers (Table 1). Specifically,  $T_{\rm g}$  values used were 84 °C for p(HNb), 89 °C for p(EtW), and 38 °C for p(DDW), based on the asymptotic  $T_{\rm g}$  value from Figure 2, and the corresponding WLF parameters are listed in Table 1.

Often, the temperature dependence of the relaxation processes of polymers near  $T_{\rm g}$  is quantified by the fragility index (m). Here, m values of the three series of polymers can be estimated using the WLF parameters,  $C_{1,\rm g}$ ,  $C_{2,\rm g}$ , with  $T_{\rm ref} = T_{\rm g}$  (Table 1)<sup>27</sup>

$$m = T_{g} \frac{C_{1,g}}{C_{2,g}} \bigg|_{T_{ref} = T_{g}}$$
(6)

Using eq 6, the values of m for p(HNb), p(EtW), and p(DDW) were estimated to be 91.1, 90.7, and 59.1, correspondingly. In comparison with p(HNb), both wedgelike polymers showed lower m values. However, a further increase of the alkyl side chain length on the wedge from ethyl to n-dodecyl significantly reduced the fragility of the wedgelike polymers. <sup>61,62,64</sup> This trend is consistent with that observed in polymers with flexible backbones: attachment of aromatic side groups raises the fragility of the polymer, whereas an increase of the length of alkyl side chain length reduces the fragility index. <sup>61</sup> For example, within the p(alkyl methacrylate) family, the fragility index decreases from a value greater than 80 to less than 40 when the alkyl chain length increases from  $C_2$  to  $C_{10}$ . Note that the p(DDW) displayed a value of m = 59, which is within the range of a typical "strong" polymer such as polyisobutylene. <sup>63,65</sup>

# CONCLUSIONS

Three series of well-defined polymers with varying degrees of polymerization of norbornene backbones and varying pendant wedge groups were synthesized. Each of the three polymer series systematically increased the size of the pendant group to determine the effect that the pendant group size had on both solution conformation and bulk melt properties of the polymers. Comparisons of these polymer series lead to three significant observations of the dynamics of these norbornene imide-based polymers. First, regardless of the pendant group, these norbornene imide-based polymers exhibit a more rodlike conformation in the solution phase than RSAW polymers. Interestingly, the pendant wedge groups increase the rodlike conformation of the polymer main chain in comparison to the hexyl side group, but the longer, n-dodecyl alkyl chain did not have as great of an effect on the conformation compared to the ethyl alkyl chain. Although, it is important to note that the persistence lengths for the p(DDW) and p(EtW) series reported here are fairly short compared to those reported for similar dendronized polymers. 16 This observation can

potentially be attributed to the structure of the dendron pendant group as well as the proximity of the branching point to the polymer backbone. However, further experimentation would help elucidate the underlying reasons for this observed difference. Second, the increased size of the pendant wedge groups increases the polymer chain diameter that leads to a dramatic increase in the molecular weight between entanglements, which can be qualitatively rationalized by the packing model. Third, the side groups had a tremendous impact on the fragility of the norbornene-imide backbone polymers. Replacing the *n*-hexyl group with ethyl-wedge side groups slightly lowered the fragility of the polymer, whereas a further increase in the alkyl side group length on the wedgelike polymer significantly reduces the fragility of the polymer. The fundamental understanding on the effects of side groups on the norbornene-based polymers will allow for molecular design of polymers with desired combinations of properties that are critical for both applications and manufacturing.

# ASSOCIATED CONTENT

# S Supporting Information

The Supporting Information is available free of charge on the ACS Publications website at DOI: 10.1021/acs.macromol.9b00020.

Materials and methods; synthetic procedures; spectroscopic results (NMR, mass spectroscopy, GPC-MALS); fractal dimensional analysis; method of density estimation in dynamic oscillatory measurements; isofrictional rheological analysis; individual DSC traces; DMA traces; and dynamic master curves (PDF)

#### AUTHOR INFORMATION

# **Corresponding Authors**

\*E-mail: Garret.Miyake@colostate.edu (G.M.M.).

\*E-mail: Yifu.Ding@Colorado.edu (Y.D.).

# ORCID (

Garret M. Miyake: 0000-0003-2451-7090

Yifu Ding: 0000-0001-7779-7781

### **Author Contributions**

§B.M.B. and O.H. co-first authorship.

#### Notes

The authors declare no competing financial interest.

#### ACKNOWLEDGMENTS

B.M.B. and G.M.M. would like to thank the Colorado State University, the National Science Foundation (CMMI-1634941), the Advanced Research Projects Agency-Energy (DEAR0000683), and the National Institute of General Medical Sciences of the National Institutes of Health under Award Number R35GM119702. The content is solely the responsibility of the authors and does not necessarily represent the official views of the National Institutes of Health. O.H. and Y.D. gratefully acknowledge the National Science Foundation (NSF) Industry/University Cooperative Research Center for Membrane Science, Engineering and Technology (MAST) at the University of Colorado at Boulder (CU-B) for support of this research via NSF Award IIP 1624602.

# REFERENCES

(1) Daniel, W. F. M.; Burdynska, J.; Vatankhah-Varnoosfaderani, M.; Matyjaszewski, K.; Paturej, J.; Rubinstein, M.; Dobrynin, A. V.;

Sheiko, S. S. Solvent-free, supersoft and superelastic bottlebrush melts and networks. *Nat. Mater.* **2016**, *15*, 183–190.

- (2) Verduzco, R.; Li, X.; Pesek, S. L.; Stein, G. E. Structure, function, self-assembly, and applications of bottlebrush copolymers. *Chem. Soc. Rev.* **2015**, *44*, 2405.
- (3) Dalsin, S. J.; Rions-Maehren, T. G.; Beam, M. D.; Bates, F. S.; Hillmyer, M. A.; Matsen, M. W. Bottlebrush Block Polymers: Quantitative Theory and Experiments. *ACS Nano* **2015**, *9*, 12233–12245.
- (4) Rzayev, J. Molecular Bottlebrushes: New Opportunities in Nanomaterials Fabrication. *ACS Macro Lett.* **2012**, *1*, 1146–1149.
- (5) Haugan, I. N.; Maher, M. J.; Chang, A. B.; Lin, T.-P.; Grubbs, R. H.; Hillmyer, H. A.; Bates, F. S. Consequences of Grafting Density on the Linear Viscoelastic Behavior of Graft Polymers. *ACS Macro Lett.* **2018**, *7*, 525–530.
- (6) Dalsin, S. J.; Hillmyer, M. A.; Bates, F. S. Linear Rheology of Polyolefin-Based Bottlebrush Polymers. *Macromolecules* **2015**, 48, 4680–4691.
- (7) Hu, M.; Xia, Y.; McKenna, G. B.; Kornfield, J. A.; Grubbs, R. H. Linear Rheological Response of a Series of Densely Branched Brush Polymers. *Macromolecules* **2011**, *44*, 6935–6943.
- (8) Aluculesei, A.; Pipertzis, A.; Piunova, V. A.; Miyake, G. M.; Floudas, G.; Fytas, G.; Grubbs, R. H. Thermomechanical Behavior and Local Dynamics of Dendronized Block Copolymers and Constituent Homopolymers. *Macromolecules* **2015**, *48*, 4142–4150.
- (9) Hsu, H.-P.; Paul, W.; Binder, K. One- and Two-Component Bottle-brush Polymers: Simulations Compared to Theoretical Predictions. *Macromol. Theory Simul.* **2007**, *16*, 660–689.
- (10) Paturej, J.; Sheiko, S. S.; Panyukov, S.; Rubinstein, M. Molecular Structure of Bottlebrush Polymers in Melts. *Sci. Adv.* **2016**, *2*, No. e1601478.
- (11) Kavassalis, T. A.; Noolandi, J. Entanglement Scaling in Polymer Melts and Solutions. *Macromolecules* **1989**, *22*, 2709–2720.
- (12) Cao, Z.; Carrillo, J.-M. Y.; Sheiko, S. S.; Dobrynin, A. V. Computer Simulations of Bottle Brushes: From Melts to Soft Networks. *Macromolecules* **2015**, *48*, 5006–5015.
- (13) Fetters, L. J.; Lohse, D. J.; Milner, S. T.; Graessley, W. W. Packing Length Influence in Linear Polymer Melts on Entanglement, Critical, and Reptation Molecular Weights. *Macromolecules* **1999**, 32, 6847–6851.
- (14) Hawker, C. J.; Frechet, J. M. J. Preparation of Polymers with Controlled Molecular Architecture. A New Convergent Approach to Dendritic Macromolecules. *J. Am. Chem. Soc.* **1990**, *112*, 7638–7647.
- (15) Percec, V.; Ahn, C.-H.; Bera, T. K.; Ungar, G.; Yeardley, D. J. P. Coassembly of a Hexagonal Columnar Liquid Crystalline Superlattice from Polymer(s) Coated with a Three-Cylindrical Bundle Supramolecular Dendrimer. *Chem. Eur. J.* 1999, 5, 1070–1083.
- (16) Zhang, B.; Wepf, R.; Fischer, K.; Schmidt, M.; Besse, S.; Lindner, P.; King, B. T.; Sigel, R.; Schurtenberger, P.; Talmon, Y.; Ding, Y.; Kroger, M.; Halperin, A.; Schluter, A. D. The Largest Synthetic Structure with Molecular Precision: Towards a Molecular Object. *Angew. Chem., Int. Ed.* **2011**, *50*, 737–740.
- (17) Karakaya, B.; Claussen, W.; Gessler, K.; Saenger, W.; Schluter, A.-D. Toward Dendrimers with Cylindrical Shape in Solution. *J. Am. Chem. Soc.* **1997**, *119*, 3296–3301.
- (18) Helms, B.; Mynar, J. L.; Hawker, C. J.; Frechet, J. M. J. Dendronized Linear Polymers via "Click Chemistry". *J. Am. Chem. Soc.* **2004**, 126, 15020–15021.
- (19) Boydston, A. J.; Holcombe, T. W.; Unruh, D. A.; Frechet, J. M. J.; Grubbs, R. H. A Direct Route to Cyclic Organic Nanostructures via Ring-Expansion Metathesis Polymerization of a Dendronized Macromonomer. *J. Am. Chem. Soc.* **2009**, *131*, 5388–5389.
- (20) Ter Huurne, G. M.; Vantomme, G.; van den Bersselaar, B. W. L.; Thota, B. N. S.; Voets, I. K.; Palmans, A. R. A.; Meijer, E. W. The Effect of Dendritic Pendants on the Folding of Amphiphilic Copolymers via Supramolecular Interactions. *J. Polym. Sci., Part A: Polym. Chem.* 2019, 411–421.

(21) Deng, J.; Zhou, Y.; Xu, B.; Mai, K.; Deng, Y.; Zhang, L.-M. Dendronized Chitosan Derivative as a Biocompatible Gene Delivery Carrier. Biomacromolecules 2011, 12, 642-649.

- (22) Li, W.; Wu, D.; Schluter, A. D.; Zhang, A. Synthesis of an Oligo(ethylene glycol)-Based Third-Generation Thermoresponsive Dendronized Polymer. J. Polym. Sci., Part A: Polym. Chem. 2009, 47, 6630-6640.
- (23) Knapen, J. W. J.; van der Made, A. W.; de Wilde, J. C.; van Leeuwen, P. W. N. M.; Wijkens, P.; Grove, D. M.; van Koten, G. Homogeneous catalysts based on silane dendrimers functionalized with arylnickel(II) complexes. Nature 1994, 372, 659-663.
- (24) Piunova, V. A.; Miyake, G. M.; Daeffler, C. S.; Weitekamp, R. A.; Grubbs, R. H. Highly Ordered Dielectric Mirrors via the Self-Assembly of Dendronized Block Copolymers. J. Am. Chem. Soc. 2013, 135, 15609-15616.
- (25) Boyle, B. M.; French, T. A.; Pearson, R. M.; McCarthy, B. G.; Miyake, G. M. Structural Color for Additive Manufacturing: 3D-Printed Photonic Crystals from Block Copolymers. ACS Nano 2017, 11, 3052-3058.
- (26) Qian, Z.; Koh, Y. P.; Pallaka, M. R.; Chang, A. B.; Lin, T.-P.; Guzman, P. E.; Grubbs, R. H.; Simon, S. L.; McKenna, G. B. Linear Rheology of a Series of Second-Generation Dendronized Wedge Polymers. Macromolecules 2019, 2063-2074.
- (27) Hu, M.; Xia, Y.; Daeffler, C. S.; Wang, J.; McKenna, G. B.; Kornfield, J. A.; Grubbs, R. H. The Linear Rheological Responses of Wedge-Type Polymers. J. Polym. Sci., Part B: Polym. Phys. 2015, 53, 899-906.
- (28) Pasquino, R.; Zhang, B.; Sigel, R.; Yu, H.; Ottiger, M.; Bertran, O.; Aleman, C.; Schluter, A. D.; Vlassopoulos, D. Linear Viscoelastic Response of Dendronized Polymers. Macromolecules 2012, 45, 8813-8823.
- (29) Costanzo, S.; Scherz, L. F.; Schweizer, T.; Kroger, M.; Floudas, G.; Schluter, A. D.; Vlassopoulos, D. Rheology and Packing of Dendronized Polymers. Macromolecules 2016, 49, 7054-7068.
- (30) Dutertre, F.; Bang, K.-T.; Loppinet, B.; Choi, I.; Choi, T.-L.; Fytas, G. Structure and Dynamics of Dendronized Polymer Solutions: Gaussian Coil or Macromolecular Rod? Macromolecules 2016, 49, 2731-2740.
- (31) Ouali, N.; Mery, S.; Skoulios, A.; Noirez, L. Backbone Stretching of Wormlike Carbosilane Dendrimers. Macromolecules 2000, 33, 6185-6193.
- (32) Graessley, W. W. The Entanglement Concept in Polymer Rheology; Springer: Berlin, 1974.
- (33) Miyake, G. M.; Weitekamp, R. A.; Grubbs, R. H. Handbook of Metathesis: Synthesis of Materials with Nanostructured Periodicity, 2nd ed.; Wiley-VCH: Weiheim, Germany, 2015.
- (34) Vougioukalakis, G. C.; Grubbs, R. H. Ruthenium-Based Heterocyclic Carbene-Coordinated Olefin Metathesis Catalysts. Chem. Rev. 2010, 110, 1746-1787.
- (35) Bielawksi, C. W.; Grubbs, R. H. Living Ring-Opening Metathesis Polymerization. Prog. Polym. Sci. 2007, 32, 1-29.
- (36) Leitgeb, A.; Wappel, J.; Slugovc, C. The ROMP Toolbox Upgraded. Polymer 2010, 51, 2927-2946.
- (37) Flory, P. J.; Fisk, S. Effect of Volume Exclusion on the Dimensions of Polymer Chains. J. Chem. Phys. 1966, 44, 2243.
- (38) Fixman, M. Radius of Gyration of Polymer Chains. J. Chem. Phys. 1962, 36, 306.
- (39) Dünweg, B.; Kremer, K. Molecular Dynamics Simulation of a Polymer Chain in Solution. J. Chem. Phys 1993, 99, 6983.
- (40) Fetters, L. J.; Lohse, D. J.; Richter, D.; Witten, T. A.; Zirkel, A. Connection between Polymer Molecular Weight, Density, Chain Dimensions, and Melt Viscoelastic Properties. Macromolecules 1994, 27, 4639-4647.
- (41) De Gennes, P. G. Scaling Concepts in Polymer Physics; Cornell University Press: London, U.K., 1979.
- (42) Benoit, H.; Doty, P. Light Scattering from Non-Gaussian Chains. J. Phys. Chem. 1953, 57, 958-963.
- (43) Marsh, D. Scaling and Mean-Field Theories Applied to Polymer Brushes. Biophys. J. 2004, 86, 2630-2633.

I

(44) Hsu, H.-P.; Paul, W.; Rathgeber, S.; Binder, K. Characteristic Length Scales and Radial Monomer Density Profiles of Molecular Bottle-Brushes: Simulation and Experiment. Macromolecules 2010, 43, 1592-1601.

- (45) Ding, Y.; Kisliuk, A.; Sokolov, A. P. When Does a Molecule Become a Polymer? Macromolecules 2004, 37, 161-166.
- (46) Floudas, G.; Stepanek, P. Structure and Dynamics of Poly(ndecyl methacrylate) below and Above the Glass Transition. Macromolecules 1998, 31, 6951-6957.
- (47) Beiner, M.; Korus, J.; Donth, E. Dynamic Glass Transition above the Cooperativity Onset in Poly(n-octyl methacrylate). Macromolecules 1997, 30, 8420-8424.
- (48) Rong, W.; Fan, Z.; Yu, Y.; Bu, H.; Wang, M. Influence of entanglements on glass transition of atactic polystyrene. J. Polym. Sci., Part B: Polym. Phys. 2005, 43, 2243.
- (49) Ngai, K. L.; Paluch, M. Classification of Secondary Relaxation in Glass-Formers based on Dynamic Properties. J. Chem. Phys. 2004,
- (50) Mirigian, S.; Schweizer, K. S. Elastically Cooperative Activated Barrier Hopping Theory of Relaxation in Viscous Fluids. II. Thermal Liquids. J. Chem. Phys. 2014, 140, No. 194507.
- (51) Sunthar, P. In Rheology of Complex Fluids; Deshpande, A. P.; Krishnan, J. M.; Kumar, S., Eds.; Springer: New York, 2010.
- (52) van Gurp, M.; Palmen, J. Time-Temperature Superposition for Polymeric Blends. Rheol. Bull. 1998, 67, 5-8.
- (53) Trinkle, S.; Friedrich, C. Van Gurp-Palmen-Plot: a way to characterize polydispersity of linear polymers. Rheol. Acta 2001, 40,
- (54) Trinkle, S.; Walter, P.; Friedrich, C. Van Gurp-Palmen Plot II classification of long chain branched polymers by their topology. Rheol. Acta 2002, 41, 103-113.
- (55) Dealy, J.; Plazek, D. Time-Temperature Superposition A User's Guide. Rheol. Bull. 2009, 78, 16-31.
- (56) Fetters, L. J.; Lohse, D. J.; Graessley, W. W. Chain Dimensions and Entanglement Spacings in Dense Macromolecular Systems. J. Polym. Sci., Part B: Polym. Phys. 1999, 37, 1023-1033.
- (57) Patel, S. K.; Malone, S.; Cohen, C.; Gillmor, J. R.; Colby, R. H. Elastic Modulus and Equilibrium Swelling of Poly(dimethylsiloxane) Networks. Macromolecules 1992, 25, 5241-5251.
- (58) Fetters, L. J.; Lohse, D. J.; Richter, D.; Witten, T. A.; Zirkel, A. Connection between Polymer Molecular Weight, Density, Chain Dimensions, and Melt Viscoelastic Properties. Macromolecules 1994,
- (59) Williams, M. L.; Landel, R. F.; Ferry, J. D. The Temperature Dependence of Relaxation Mechanisms in Amorphous Polymers and Other Glass-Forming Liquids. J. Am. Chem. Soc. 1955, 77, 3701-
- (60) Ferry, J. D. In Visoelastic Properties of Polymers, 3rd ed.; Ferry, J. D., Ed.; John Wiley & Sons: New York, 1980; p 304.
- (61) Kunal, K.; Robertson, C. G.; Pawlus, S.; Hahn, S. F.; Sokolov, A. P. Role of Chemical Structure in Fragility of Polymers: A Qualitative Picture. Macromolecules 2008, 41, 7232-7238.
- (62) Ding, Y.; Sokolov, A. P. Breakdown of Time-Temperature Superposition Principle and Universality of Chain Dynamics in Polymers. Macromolecules 2006, 39, 3322-3326.
- (63) Ngai, K. L.; Roland, C. M. Chemical Structure and Intermolecular Cooperativity: Dielectric Relaxation Results. Macromolecules 1993, 26, 6824-6830.
- (64) He, X.; Wu, J.; Huang, G.; Wang, X. Effect of Alkyl Side Chain Length on Relaxation Behaviors in Poly(n-alkyl Acrylates) and Poly(n-alkyl Methacrylates). J. Macromol. Sci., Part B 2010, 50, 188-
- (65) Angell, C. A. Relaxation in liquids, polymers and plastic crystals - strong/fragile patterns and problems. J. Non-Cryst. Solids 1991, 131-133, 13-31.